Second harmonic study of thermally oxidized mono- and few-layer 2*H*-MoS_2

Katharina Burgholzer,[1,*,†] Henry Hübschmann,[2,3,4,*,‡] Gerhard Berth,[2,3,4] Adriana Bocchini,[2,3,4] Uwe Gerstmann,[2,4] Wolf Gero Schmidt,[2,4] Rajdeep Adhikari,[1,5] Klaus D. Jöns,[2,3,4] and Alberta Bonanni[1]

[1]*Institute of Semiconductor and Solid State Physics, Johannes Kepler University Linz, 4040 Linz, Austria*

[2]*Department of Physics, Paderborn University, 33095 Paderborn, Germany*

[3]*Institute for Photonic Quantum Systems, Paderborn University, 33095 Paderborn, Germany*

[4]*Center for Optoelectronics and Photonics Paderborn, Paderborn University, 33095 Paderborn, Germany*

[5]*Linz Institute of Technology, Johannes Kepler University Linz, 4040 Linz, Austria*

(Received 9 March 2026; revised 17 July 2026; accepted 20 July 2026; published 17 August 2026)

A comprehensive study of second harmonic generation on thermally oxidized MoS_2 flakes with the thickness ranging from monolayer up to seven layers is presented. Observing the fundamental nonlinear behavior for nontreated and oxidized MoS_2 reveals that oxidation causes significant changes in the second harmonic response for all investigated structures. Excitation-power-dependent measurements to analyze the nonlinear behavior with respect to the oxidation time show progressive oxidation within the maximum oxidation time of 6 h under the considered oxidation conditions. Here, polarization-dependent measurements reveal the structural changes due to oxidation. Additionally, it is found that the oxidation depth is restricted to the topmost S layer and the oxidation behavior exhibits a layer dependency. These findings are supported by theoretical band structure calculations. The results demonstrate that the thermal oxidation progress of two-dimensional MoS_2 can be monitored with nonresonant and noninvasive SH microscopy by following the distinct fingerprints of structural modification in the nonlinear response.

DOI: 10.1103/7n6z-9tsr

I. INTRODUCTION

Two-dimensional (2D) semiconductors belonging to the family of transition metal dichalcogenides have attracted increasing attention as building blocks for next-generation nanoelectronics. In particular, molybdenum disulfide (MoS_2), in addition to showing an electron mobility up to 200 $cm^2\,V^{-1}s^{-1}$ [1], has a thickness-dependent band structure and a band gap ranging from an indirect gap of 1.2 eV in the bulk state [2] to a direct gap of 1.8 eV in monolayer form [3] at room temperature. For this reason, MoS_2 is already being applied in atomically thin devices for nanoelectronics [1,4], photovoltaics and photodetection [5,6], chemical sensorics [7,8], and electrochemical catalysis [9]. Thermal oxidation is involved in the fabrication of such devices in order to tune their electronic and optical properties [4]. A comprehensive understanding of the thermal oxidation mechanism of MoS_2 is crucial to ensure the reliability and optimized performance of MoS_2-based devices. Since an odd number of 2*H*-MoS_2 layers exhibits no inversion symmetry and gives rise to second-order optical nonlinearity ($\chi^{(2)} \neq 0$) and the structural impact of oxidation is expected, second harmonic (SH) microscopy is a helpful tool for analyzing the crystal structure and changes due to oxidation. Here, a comprehensive study is conducted on how oxidation affects the nonlinear optical response of 2*H*-MoS_2 flakes with thickness ranging from one layer (1L) up to 7L on SiO_2.

II. MATERIAL SYSTEM

A. Crystal symmetry

Monolayer (1L) MoS_2 contains two hexagonal S lattices with a layer of Mo atoms positioned in trigonal prismatic coordination between the S planes, leading to the crystal structure with broken inversion symmetry shown in Fig. 1. Monolayer MoS_2 belongs to the D_{3h} symmetry group, with only one independent, nonvanishing nonlinear tensor element, $d_{yyy} = -d_{yxx} = -d_{xxy} = -d_{xyx}$, along the high-symmetry directions, armchair and zigzag, each with threefold symmetry. For bilayer (2L) 2*H*-MoS_2 another S-Mo-S layer is added with AA' stacking [10], resulting in a centrosymmetric D_{3d} space group. Consequently, for an odd number of layers the inversion symmetry is broken, whereas for an even number the inversion symmetry is restored [11].

B. Sample fabrication

The investigated MoS_2 samples were fabricated by mechanical exfoliation [12] from a bulk 2*H*-MoS_2 crystal obtained from MaTeck. For the first inspection and the following transfer step, the MoS_2 flakes were placed onto viscoelastic polydimethylsiloxane (PDMS) stamps with a rigid metallic

*These authors contributed equally to this work.
†Contact author: katharina.burgholzer@jku.at
‡Contact author: henry.volker.huebschmann@uni-paderborn.de

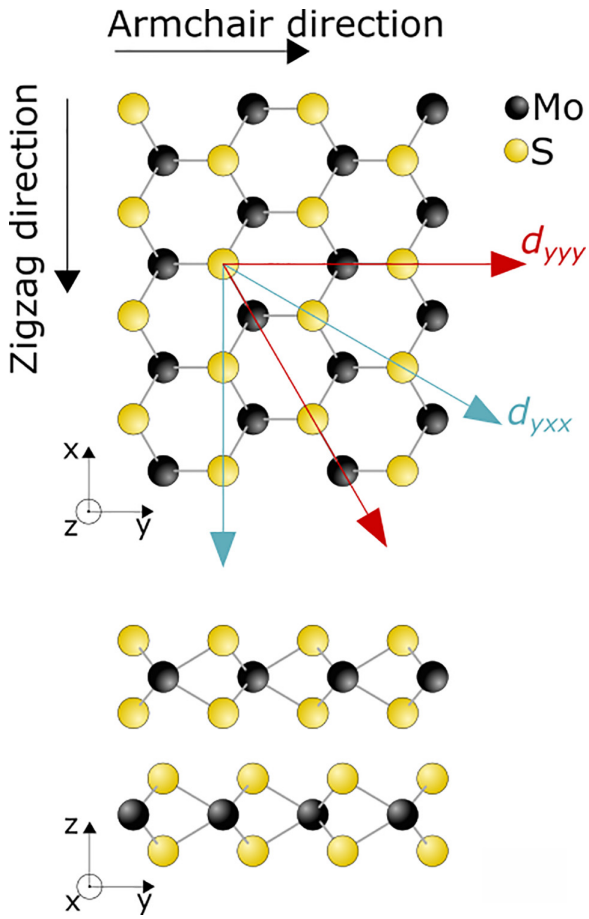

FIG. 1. Crystal structure of 2*H*-MoS_2: top view with indications of the armchair and zigzag directions and corresponding orientation of the nonlinear tensor elements d_{yyy} and d_{yxx} (top) and side view of the 2*H* stacking (bottom).

support. Suitable MoS_2 flakes were transferred onto Si substrates covered with 285 nm of SiO_2 using a custom deterministic all-dry transfer setup. To avoid full oxidation, preliminary tests at various temperatures were carried out, and the specimens were monitored under an optical microscope and by x-ray photoemission spectroscopy. These tests showed that 300 °C is the temperature of choice for visible oxidation of the chosen material configuration without destroying the crystal structure, in agreement with previous studies [13]. Therefore, in the last fabrication step, the samples were heated to $T = 300\,^{\circ}\mathrm{C}$ with a ramp time of 200 s and annealed for different times $t_a = 0, 2, 4, 6$ h in a MILA-5000 infrared lamp heating system with controlled O flow of 15 sccm throughout the thermal oxidation process.

C. Precharacterization

The determination of the shape and thickness of few-layer MoS_2 was performed with a high-resolution Keyence VHX-7000 optical microscope. In the optical images structural defects, e.g., wrinkles, are visible. Furthermore, the contact between the flake and the substrate can be ensured. Up to nine MoS_2 layers can be identified by comparing the contrast and color [14]. All structures were inspected before and after

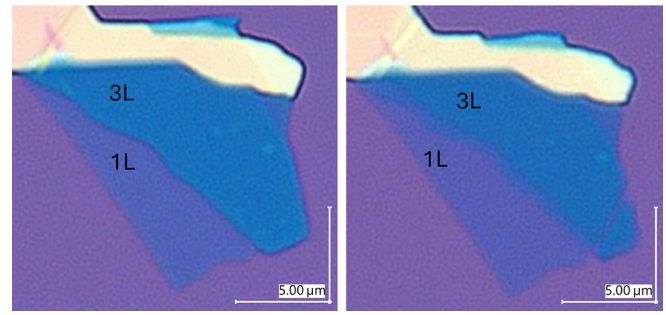

FIG. 2. Optical images of MoS_2 flakes on the SiO_2/Si substrate before (left) and after (right) 6 h oxidation at 300 °C. Here, the regions for the 1L and 3L systems are labeled. Structural modifications due to oxidation become visible in the slight change in contrast. Especially at the edges of regions with different thicknesses, a significant modification is observed.

oxidation with respect to macroscopic structural modifications induced by annealing and O exposure. Exemplary images of one sample with a 1L region and a 3L region before and after 6 h oxidation are shown in Fig. 2. The thermal oxidation treatment of MoS_2 flakes induces a slight change in contrast, as evidenced by the comparison between the 1L and 3L areas in Fig. 2. Furthermore, partially damaged areas and highly oxidized MoS_2 can be discerned. Especially at the edges of regions with different thicknesses and at the defects, a significant modification is observed, likely due to dangling bonds at the edges [13]. For further analysis, only regions which appear homogeneous in the optical images are considered.

The individual layer-number-dependent optical contrast of untreated MoS_2 flakes is calibrated via Raman spectroscopy [15]. The determination of the layer numbers relies primarily on the evolution of the Raman shift of the two dominant Raman modes, E^1_{2g} and A_{1g}, which are red- and blueshifted, respectively, with increasing layer number. To avoid systematic disturbances, the more stable absolute Raman shift difference between the two phonon modes is considered and is plotted in Fig. 3 as a function of the layer number. Due to the convergence to the bulk Raman shift of each phonon mode [15], the absolute Raman shift difference also converges for an increasing number of layers. Thus, Raman analysis is reliable for layer numbers up to 5L. For a higher layer number, additional information is required to determine the thickness, e.g., whether there is an even or odd number of layers, which can be evidenced by the SH intensity, which will be discussed later. In this work, the analyzed nonoxidized and oxidized sample thickness ranges from 1L to 7L.

III. METHODS

A. Experimental environment

The nonlinear analysis presented in this work was conducted with a custom-built nonlinear optical setup which allows for power- and polarization-controlled measurements. The excitation light from a Toptica FemtoFiber Smart 780 pulsed laser (central wavelength of 783 ± 5 nm, 100 fs pulse duration, 80 MHz repetition rate) was focused onto the sample through an infinite corrected objective (numerical aperture

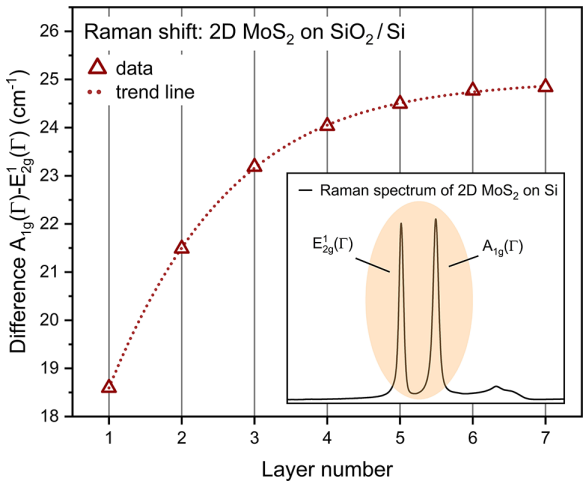

FIG. 3. Absolute Raman shift difference progression with layer number for MoS_2 on the SiO_2/Si substrate. The shift difference is taken between phonon modes $E^1_{2g}(\Gamma)$ and $A_{1g}(\Gamma)$, which undergo a redshift (blueshift) with increasing layer number, respectively.

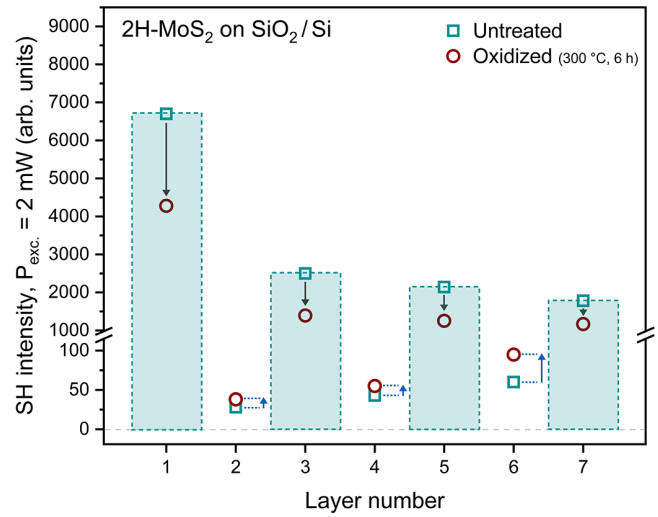

FIG. 4. Absolute SH signal for untreated and oxidized 2*H*-MoS_2 samples with respect to the layer number. Changes due to oxidation are indicates by arrows. Measurements are performed at 2 mW laser power and 1 s integration time.

of 0.95, 100× magnification). The generated SH-light was collected by the same objective in the backscattering direction and detected by a single-photon counting module (silicon avalanche photodiode). For spectral filtering (to avoid detection of excitation light), a dichroic beam splitter and appropriate color filters were implemented. In the framework of a fixed laser focus the sample positioning was realized by a three-dimensional positioning unit. Due to the unknown orientation of the MoS_2 flakes with respect to the laboratory frame, identification of the individual crystal axes is essential. To obtain full orientation information, the incident laser polarization is defined via a half-wave plate, and the detection polarization is specified by using a pol-analyzer. Simultaneous rotation of both allows for scanning the sixfold symmetry of one specific tensor element. If the polarization of the incident laser is perpendicular to the detection polarization, the zigzag direction corresponding to d_{yxx} is detected, and if they are parallel aligned, the armchair direction d_{yyy} is probed. Polar plots are reported in the laboratory frame; because the in-plane crystal orientation of each flake relative to the laboratory axes is arbitrary and different flakes are used for different oxidation times, datasets can exhibit a constant angular offset. This offset is unrelated to oxidation and does not reflect a physical rotation of the crystal axes. In this work, the acquisition of the SH intensity was performed in the parallel polarization orientation in alignment with the corresponding crystal axis due to the equivalence of the absolute values of the two tensor elements.

B. Computational environment

Ground-state crystal geometries and electronic structures were obtained within density functional theory (DFT), as implemented in the open-source program package QUANTUM ESPRESSO [16,17]. The spin-orbit coupling (SOC) is neglected in the calculations, and only the fully oxidized case is considered; i.e., the top S layer is fully substituted by O atoms.

To model the oxidized MoO_xS_{2-x} few-layer systems under periodic boundary conditions, the lattice parameters $a = b =$ 3.163 Å were kept fixed at the experimental value [18] of MoS_2, and about 10 Å of vacuum were added along the [001] crystal direction on up to 3L of MoS_2. The atomic positions, on the other hand, were relaxed until the fluctuations of forces and the total energy were below 10^{-8} Ry/bohr and 10^{-4} Ry, respectively. In addition, plane waves were expanded up to an energy cutoff of 90 Ry, and the Brillouin zone was sampled using a Γ-centered $12 \times 12 \times 1$ $\boldsymbol{k}$-point mesh.

The electronic exchange and correlation effects were modeled within the generalized gradient approximation using the Perdew-Burke-Ernzerhof functional [19]. In addition, norm-conserving pseudopotentials were employed, and the van der Waals interactions were accounted for via the semiempirical Grimme D3 scheme [20].

IV. NONLINEAR ANALYSIS

A. Layer-dependent second harmonic generation response

To study the influence of thermal oxidation on the nonlinear optical behavior of the samples, a layer-dependent analysis is performed. Specifically, untreated and oxidized (6 h at 300 °C) samples are probed, and the corresponding SH signals for different layer configurations are compared, as reported in Fig. 4, where the SH intensity as a function of the layer number is displayed for the untreated and oxidized cases.

In the untreated case, a nonlinear signal for all configurations with odd layer number parity is observed. It is due to the lack of inversion symmetry, enabling second harmonic generation (SHG). Furthermore, it becomes apparent that for the odd-layer configurations, the SH signal decreases with increasing layer number in a nonlinear manner. This behavior is attributed to the increase of absorption and changes in the band structure with increasing sample thickness ($E_{\mathrm{SHG}} > E_{\mathrm{gap}}$ for two or more layers) [21,22], here resulting in a quenched light-matter interaction [23].

For even-numbered layer configurations, no SH light is expected due to the inversion symmetry of the 2*H* AA'-stacked systems [24]. Nevertheless, a residual signal (orders of magnitude lower than the one from the odd-numbered configurations) is observed which increases with increasing layer number. The signal is likely to originate from interlayer effects [25] or from changing interlayer bonding lengths caused by the substrate and resulting in a breaking of symmetry [26]. An inherent asymmetry therefore leads to an increase of the observed SH signal for increasing layer numbers, as more material is available for SHG.

Compared to the untreated case, oxidation causes significant changes in the SH response for all layer structures. In the case of even-layer structures, the perfect inversion symmetry is broken by the higher amount of O in the topmost layer, so a relevant SH signal is introduced in the previously SHG-silent structures [27]. The case of odd-layer structures, however, is more involved and cannot be explained by simple symmetry arguments alone. We observe a reduction to about 50% to 70% for every layer number, suggesting a qualitative change (moderate reduction) in the SHG (1) by the lighter, not as easy to polarize O atoms, (2) due to clusters with local inversion symmetry, and/or (3) by oxygen-induced changes in the electronic structure.

For a better understanding of the signal change induced by oxidation, the band structures of 1L–3L of MoS_2 are calculated and plotted in Fig. 5, where the band structure of the pristine case (left) is compared with a fully oxidized top S layer (topmost S atoms substituted with O; right). For a 1L structure the oxygen-induced change in the band structure is most pronounced: The bands at the *K* point hosting the direct band gap for a pristine MoS_2 monolayer are downward shifted by more than 1 eV. A similar shift is observed at the Γ point, but here, the shift is restricted to the conduction bands, resulting in a transition from a direct to an indirect band gap. As a result, the fundamental gap is reduced to less than 0.5 eV. Interestingly, the curvature of the topmost valence band between the *M* and *K* points and, in particular, the lowest conduction bands around the Γ point is also affected and essentially flattened. As a result, the previously characteristic identical dispersion of the valence band maximum and conduction band minimum with an energy difference of about 3.16 eV (corresponding to 2×1.58 eV photon energy) is lifted, suggesting a considerable decrease in the combined density of states, providing a natural explanation for the observed O-induced decrease in SHG intensity. In other words, the behavior of an oxidized multilayer system does not resemble a system with one oxidized layer at the top and pristine layers beneath, but rather a coupled system modified by the oxidized interface at the surface. Therefore, the nonlinear response of an odd number of layers is not necessarily weakened due to oxidation in general but is presumably shifted spectrally and strongly influenced by band bending, which is expressed by a decreased SHG signal at the experimentally used center wavelength of 783 nm (1.58 eV photon energy).

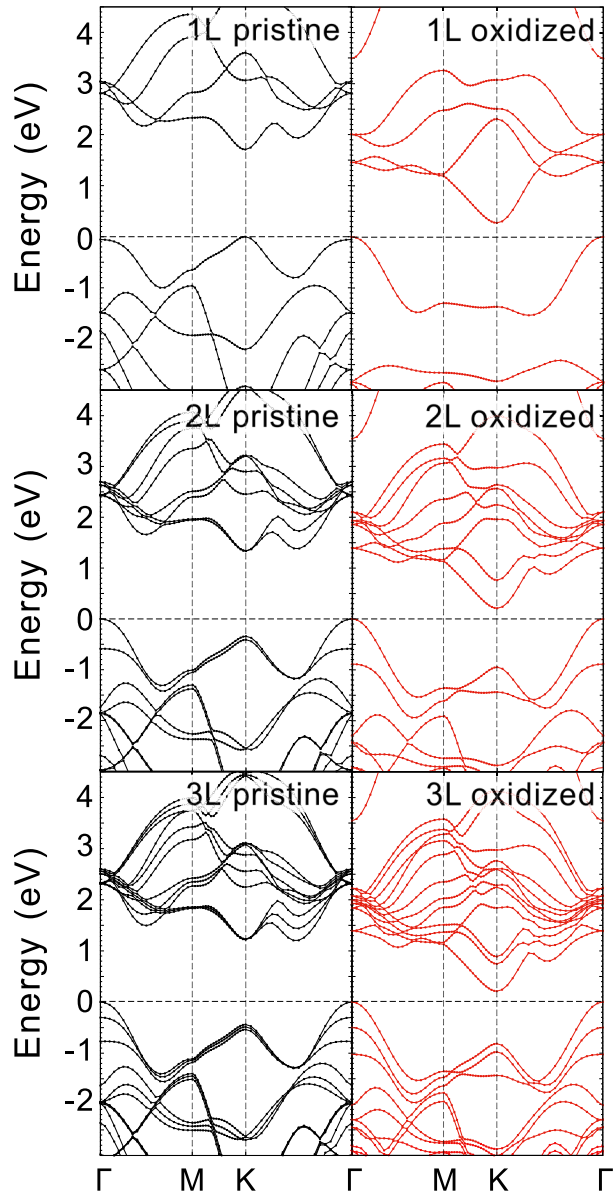

FIG. 5. DFT band structure for 1L–3L pristine MoS_2 and the influence of full substitution of the top S layer with O atoms (oxidized). With a coupling constant of $\lambda = 75$ meV [28,29], the effect of SOC is small in comparison with the changes introduced by oxidization and thus can be safely neglected here.

B. Power and polarization dependency

In the next step the nonlinear behavior with respect to oxidation time $t_a = 0, 2, 4, 6$ h is analyzed in order to prove the progress of oxidation. Here, excitation power (0–6 mW) dependent measurements are performed for each layer configuration. In order to corroborate the power-dependent results, comparative polarization-resolved measurements in the armchair direction (d_{yyy}) are carried out on untreated and 6 h oxidized MoS_2 for up to 7L. For all polarization-resolved measurements, an excitation power of 1 mW is applied to prevent laser-induced structural modifications. The fundamentally different nonlinear behaviors of even and odd numbers of layers are discussed separately, starting with odd layers.

As already observed in the layer-dependent trend in SHG intensity at fixed incident power, the SH intensity decreases

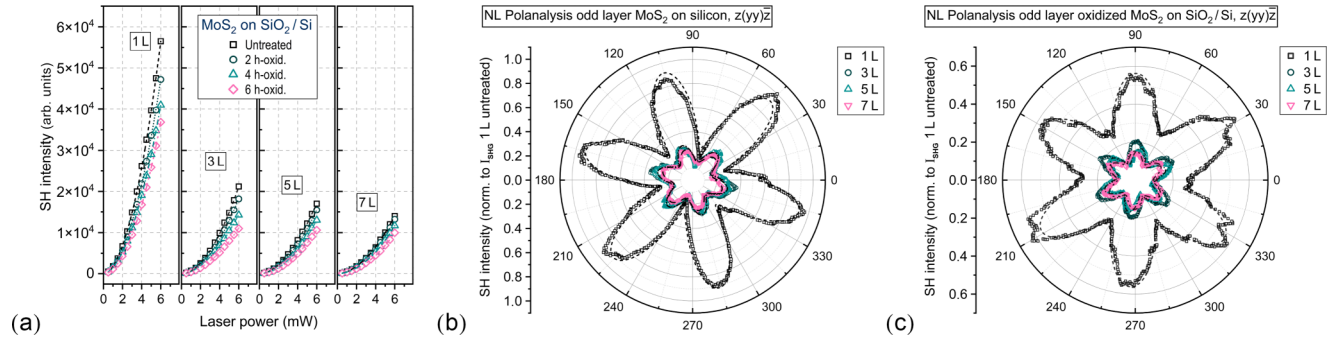

FIG. 6. (a) Power-dependent measurements showing the progression of the SH intensities with laser power for the odd-layer configurations. The measurements are separated for each layer with corresponding SH intensity progression after 0, 2, 4, and 6 h oxidation time. Polarization-dependent nonlinear analysis of odd-layer 2D MoS_2 (b) without and (c) with a 6 h oxidation treatment applied. The observed signal is normalized to the maximum intensity from 1L, with an arbitrary angle offset between the datasets. The data were obtained for 1 mW laser power with an angular resolution of 0.5°.

with increasing layer number for odd-numbered configurations. This behavior is found for every individual level of oxidation, as plotted in Fig. 6(a), where the progression of the SH intensity with laser power for odd-numbered 1L–7L MoS_2 is shown. Furthermore, the SH intensity decreases consistently with rising oxidation time for each layer configuration. This indicates a progressive oxidation within the maximum oxidation time of 6 h, but there is a strong SH signal after every oxidation time. In fact, similar studies on 1L and 2L were performed in which the SH response was probed for different degrees of oxidation but using oxygen plasma [30]. In that case, a distinct layer-by-layer conversion of MoS_2 to MoO_3 was observed. The signatures of full layer oxidation are a lost SH signal from the 1L and a strong signal from the 2L, comparable to the pristine MoS_2 1L due to the introduced lack of inversion symmetry. Although we observe a strong change in the nonlinear response after oxidation, the magnitude of the change is not in the expected range for a full change in symmetry conditions. Therefore, we predict an oxidation depth no deeper than the first sulfur layer for our thermal oxidation treatment. Additionally, the absolute decrease of SH intensity due to oxidation is reduced for increasing layer numbers. In the polarization-dependent SH intensity, a sixfold dependency arises, as shown in Fig. 6, where the SH intensity without [Fig. 6(b)] and with [Fig. 6(c)] 6 h oxidation treatment as a function of the polarization direction is displayed. After oxidation, the sixfold geometry is retained, including the respective reduction of the nonlinear signal. Furthermore, the difference between the maximum and minimum intensities decreases in the oxidized case, which indicates that the oxidation has a specific preferred direction, also possibly dependent on the number of layers [31].

The power-dependent SHG analysis for even-numbered configurations, shown in Fig. 7(a), exhibits behavior opposite that of odd layers induced by oxidation. For each untreated configuration, the SH intensity increases with incident laser power. The oxidation leads to an increase of the SH response with treatment time for every layer configuration, pointing to an ongoing oxidation process. Compared to corresponding odd-numbered configurations (e.g., comparing 6L to 5L), the resulting SH signal after 6 h oxidation for an even-numbered configuration is still an order of magnitude lower. Thus, again, full oxidation of the topmost layer can be excluded, and oxidation is confined to the surface region. In addition, each individual SH signal for a specific oxidation level (0, 2, 4, and 6 h at a specific laser power) increases with increasing layer number, whereby for all oxidation parameters (including the untreated case) the evolution of the signal occurs in a nonlinear manner.

In Fig. 7, the SH intensity for even-numbered layers is shown without [Fig. 7(b)] and with [Fig. 7(c)] a 6 h oxidation treatment applied as a function of the polarization direction. Nonoxidized even-numbered layers give no angle-dependent polarization, in accordance with the inversion symmetry. Only the residual signal is detected. Upon oxidation, sixfold symmetry of the induced polarization is found. Oxidation converts the top S plane into an oxide lacking any long-range order, while the underlying MoS_2 lattice retains its crystallinity. Accordingly, SHG arises from the crystalline MoS_2 beneath, while the top Mo-O layer breaks inversion symmetry in the even-layer 2*H* stacks, leading to the observed sixfold pattern of the induced polarization. The amorphous oxide layer is effectively isotropic and merely acts as the symmetry-breaking overlayer. The sixfold polarization dependency is inherent proof of the breaking of inversion symmetry in the system induced by the oxidation treatment and therefore supports the previously performed power-dependent analysis. It is worth emphasizing that the polarization dependency before and after oxidation is measured at the same laser power; therefore, the sixfold pattern can originate only from the O treatment.

C. Influence of oxidation time

In order to gain deeper insight into the oxidation process, the relative change in SH intensity for each number of layers is considered. The time for oxidation of the flakes is up to 6 h since longer exposures at 300 °C under 15 sccm of O_2 result in edge etching, blistering, and partial flake loss. In the chosen reaction-controlled regime, the SHG evolution is within the linear regime, consistent with the self-limiting oxidation confined to the top chalcogen plane. Although the change in the absolute SH signal for even and odd layers is quite different, the relative change in SH intensity is greater the lower the number of layers is for both sets of layer number parities.

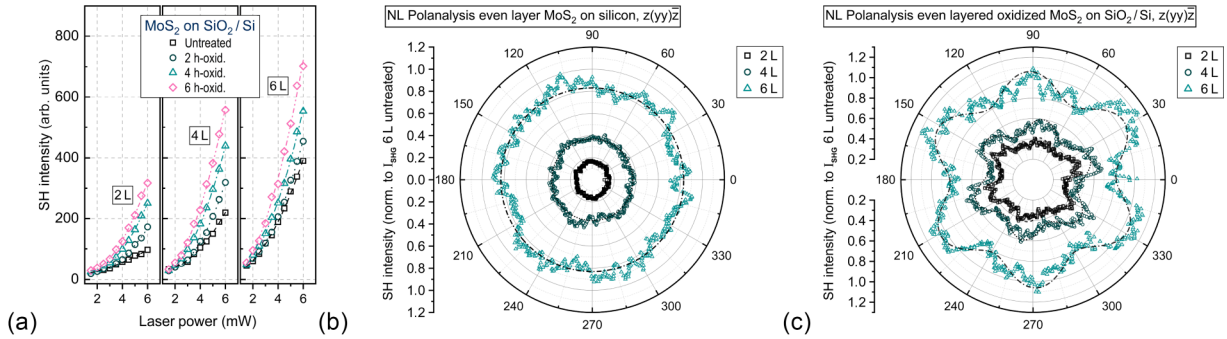

FIG. 7. (a) Progression of the SH intensities with laser power for even-layer configurations with corresponding SH intensity evolution after 0, 2, 4, and 6 h oxidation time. Polarization-dependent nonlinear analysis of even-layer 2D MoS_2 (b) without and (c) with a 6 h oxidation treatment applied. The observed signal is normalized to the maximum intensity from 6L, with an arbitrary angle offset between the datasets. The data were obtained for 1 mW laser power with an angular resolution of 0.5°.

This specific layer-dependent effect is highlighted in Fig. 8, where the oxidation-time-dependent relative change in the SH intensity is normalized to the untreated case and depicted for every odd- [Fig. 8(a)] and even-layer [Fig. 8(b)] configuration.

The relative SH signal at a fixed laser power with increasing oxidation time is approximately linear for each layer number, with the exception of the 1L, which is a special case that will be discussed later. The increasing binding energies with increasing layer number [32] result in an enhancement of the energy threshold for oxidation. For this reason the oxidation process for thicker MoS_2 configurations is less pronounced under the chosen treatment parameters, which is also observed with other analytic methods [31]. Furthermore, the calculations suggest that the modifications of the band structure by oxidation are more pronounced for 1L and 2L and show weaker changes for higher layer numbers. For the 1L, the calculation of the band structure plotted in Fig. 5 shows a transition from a direct to an indirect band gap for full oxidation of the topmost sulfur layer, resulting in a pronounced change in the SH intensity. Furthermore, the 1L behavior is influenced by the chosen substrate because of its direct contact with the substrate [33]. For SiO_2, the 1L is more stable than a higher number of layers due to the higher energy barrier for the MoS_2-substrate interface in comparison to the MoS_2-MoS_2 multilayer interface [34]. However, the high surface-to-volume ratio of the 1L counteracts this behavior, which becomes relevant for high defect rates like for S vacancies at the surface and/or sufficiently high oxidation temperature, which overcome the energy barrier introduced by the substrate.

V. SUMMARY

The thermal oxidation process of atomically thin MoS_2 was investigated utilizing SH microscopy. For this purpose, MoS_2 flakes were fabricated by mechanical exfoliation and thermally oxidized in a controlled O-rich environment for different lengths of time. The samples were inspected by optical microscopy, and the layer thickness was determined using Raman spectroscopy, which revealed MoS_2 flakes ranging

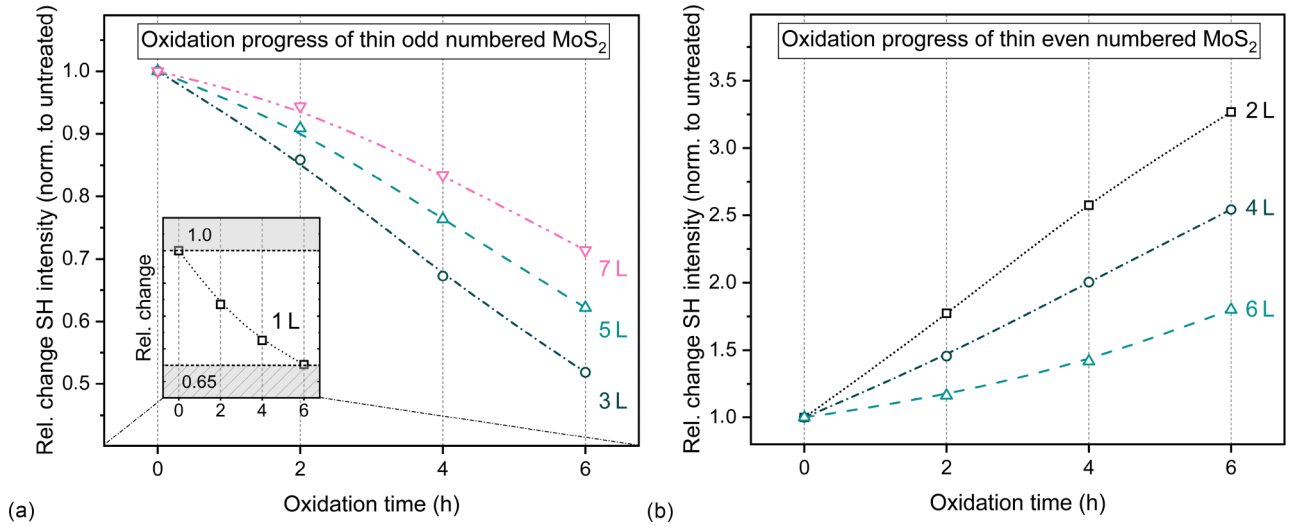

FIG. 8. Oxidation-induced relative change in the SH intensity normalized to the untreated case (laser excitation at 2 mW) with respect to the treatment time for (a) odd- and (b) even-layer configurations. Due to its fundamental different evolution the 1L configuration is individually plotted in the inset in (a).

from 1L to 7L. In the first nonlinear analysis, the layer-dependent SHG responses for untreated and oxidized samples were compared. Here, for odd-numbered MoS_2, in addition to the typical thickness dependency, a specific SH decrease was found. It is caused by oxidation attributed to distinct changes in the band structure combined with a reduction in the effective crystal available for SHG. For even-numbered structures, which show only a residual signal, oxidation leads to an enhancement of the SH signal due to the breaking of symmetry. Additionally, calculations of the band structure of 1L–3L MoS_2 for full substitution of the top S layer with O atoms were carried out, showing significant modulation with oxidation, especially for the 1L, where the band gap transitions from direct to indirect. Moreover, the nonlinear behavior with respect to the oxidation time ($t_a = 0$–6 h) in excitation-power-dependent measurements was analyzed. The ongoing decrease of the SH intensity for an odd number of layers (and the increase for an even number of layers) with increasing oxidation time indicates progressive oxidation within the maximum oxidation time of 6 h, and full oxidation of the topmost MoS_2 layer can be excluded. For an odd number of layers, a polarization-dependent analysis revealed the sixfold dependency of the SH intensity. With oxidation, the difference between the maximum and minimum intensities decreases, while the symmetry is retained. Nonoxidized even-numbered layers do not display angle-dependent polarization intensity, and only the residual signal is detected. Upon oxidation, a sixfold symmetry arises, which is evidence of the breaking of inversion symmetry by thermal oxidation. Furthermore, a thickness-dependent oxidation behavior is observed. The lower the layer number is, the more O atoms are introduced in the crystal, with the monolayer representing a special case due to its direct contact with the substrate.

In conclusion, nonresonant, noninvasive SH spectroscopy enables monitoring of thermal oxidation in one- to seven-layer MoS_2 by resolving distinct nonlinear optical fingerprints of structural modification. We further provided an exemplary analysis to estimate the degree of oxidation—covering both intentional and unintentional oxidation—in the studied samples. Together, these results reveal a layer-number-dependent oxidation pathway and offer practical guidance for the rational design and deployment of MoS_2-based devices, in line with material systems used in real applications [6,35].

ACKNOWLEDGMENTS

This work is supported by the Deutsche Forschungsgemeinschaft (DFG, German Research Foundation)–SFB-Geschäftszeichen Grant No. TRR142/3-2022–Projektnummer Grant No. 231447078) and co-funded by the European Union (ERC, LiNQs, Grant No. 101042672). K.D.J. acknowledges funding from the Ministry of Culture and Science of North Rhine-Westphalia for the Institute for Photonic Quantum Systems (PhoQS). R.A. acknowledges funding from the Austrian Science Fund (FWF) through Project No. TAI-817 and from the JKU LIT Seed Funding through Project No. LIT-2022-11-SEE-119. We also thank the Paderborn Center for Parallel Computing (PC^2) for grants of high-performance computational time.

DATA AVAILABILITY

There are no publicly available research data or software supporting this manuscript. Requests for further information or data should be sent to the authors.

[1] B. Radisavljevic, A. Radenovic, J. Brivio, V. Giacometti, and A. Kis, Single-layer MoS_2 transistors, Nat. Nanotechnol. **6**, 147 (2011).

[2] K. K. Kam and B. A. Parkinson, Detailed photocurrent spectroscopy of the semiconducting group VI transition metal dichalcogenides, J. Phys. Chem. **86**, 463 (1982).

[3] K. F. Mak, C. Lee, J. Hone, J. Shan, and T. F. Heinz, Atomically thin MoS_2: A new direct-gap semiconductor, Phys. Rev. Lett. **105**, 136805 (2010).

[4] M. Wang, S. Cai, C. Pan, C. Wang, X. Lian, Y. Zhuo, K. Xu, T. Cao, X. Pan, B. Wang, S. J. Liang, J. J. Yang, P. Wang, and F. Miao, Robust memristors based on layered two-dimensional materials, Nat. Electron. **1**, 130 (2018).

[5] M. Amani, D.-H. Lien, D. Kiriya, J. Xiao, A. Azcatl, J. Noh, S. R. Madhvapathy, R. Addou, S. KC, M. Dubey, K. Cho, R. M. Wallace, S.-C. Lee, J.-H. He, J. W. Ager, X. Zhang, E. Yablonovitch, and A. Javey, Near-unity photoluminescence quantum yield in MoS_2, Science **350**, 1065 (2015).

[6] Z. Yin, H. Li, H. Li, L. Jiang, Y. Shi, Y. Sun, G. Lu, Q. Zhang, X. Chen, and H. Zhang, Single-layer MoS_2 phototransistors, ACS Nano **6**, 74 (2012).

[7] H. Li, Z. Yin, Q. He, H. Li, X. Huang, G. Lu, D. W. H. Fam, A. I. Y. Tok, Q. Zhang, and H. Zhang, Fabrication of single- and multilayer MoS_2 film-based field-effect transistors for sensing NO at room temperature, Small **8**, 63 (2012).

[8] F. K. Perkins, A. L. Friedman, E. Cobas, P. M. Campbell, G. G. Jernigan, and B. T. Jonker, Chemical vapor sensing with monolayer MoS_2, Nano Lett. **13**, 668 (2013).

[9] Z. Wang, Q. Li, H. Xu, C. Dahl-Petersen, Q. Yang, D. Cheng, D. Cao, F. Besenbacher, J. V. Lauritsen, S. Helveg, and M. Dong, Controllable etching of MoS_2 basal planes for enhanced hydrogen evolution through the formation of active edge sites, Nano Energy **49**, 634 (2018).

[10] J. He, K. Hummer, and C. Franchini, Stacking effects on the electronic and optical properties of bilayer transition metal dichalcogenides MoS_2, $MoSe_2$, WS_2, and WSe_2, Phys. Rev. B **89**, 075409 (2014).

[11] A. Molina-Sánchez, K. Hummer, and L. Wirtz, Vibrational and optical properties of MoS_2: From monolayer to bulk Surf. Sci. Rep. **70**, 554 (2015).

[12] K. S. Novoselov, D. Jiang, F. Schedin, T. J. Booth, V. V. Khotkevich, S. V. Morozov, and A. K. Geim, Two-dimensional atomic crystals, Proc. Natl. Acad. Sci. USA **102**, 10451 (2005).

[13] Y. Jiang, Z. Liu, H. Zhou, A. Sharma, J. Deng, and C. Ke, Physical adsorption and oxidation of ultra-thin MoS_2 crystals: Insights into surface engineering for 2D electronics and beyond, Nanotechnology **34**, 405701 (2023).

[14] A. Castellanos-Gomez, N. Agrat, and G. Rubio-Bollinger, Optical identification of atomically thin dichalcogenide crystals, Appl. Phys. Lett. **96**, 213116 (2010).

[15] C. Lee, H. Yan, L. E. Brus, T. F. Heinz, J. Hone, and S. Ryu, Anomalous lattice vibrations of single- and few-layer MoS_2, ACS Nano **4**, 2695 (2010).

[16] P. Giannozzi *et al.*, QUANTUM ESPRESSO: A modular and open-source software project for quantum simulations of materials, J. Phys.: Condens. Matter **21**, 395502 (2009).

[17] P. Giannozzi *et al.*, Advanced capabilities for materials modelling with QUANTUM ESPRESSO, J. Phys.: Condens. Matter **29**, 465901 (2017).

[18] D. Fan, J. Xu, M. Ma, J. Liu, and H. Xie, *P–V–T* equation of state of molybdenite (MoS_2) by a diamond anvil cell and *in situ* synchrotron angle-dispersive X-ray diffraction, Physica B **451**, 53 (2014).

[19] J. P. Perdew, K. Burke, and M. Ernzerhof, Generalized gradient approximation made simple, Phys. Rev. Lett. **77**, 3865 (1996).

[20] S. Grimme, J. Antony, S. Ehrlich, and H. Krieg, A consistent and accurate *ab initio* parametrization of density functional dispersion correction (DFT-D) for the 94 elements H-Pu, J. Chem. Phys. **132**, 154104 (2010).

[21] A. Castellanos-Gomez, J. Quereda, H. P. van der Meulen, N. Agraït, and G. Rubio-Bolinger, Spatially resolved optical absorption spectroscopy of single- and few-layer MoS_2 by hyperspectral imaging, Nanotechnology **27**, 115705 (2016).

[22] N. Kumar, S. Najmaei, Q. Cui, F. Ceballos, P. M. Ajayan, J. Lou, and H. Zhao, Second harmonic microscopy of monolayer MoS_2, Phys. Rev. B **87**, 161403(R) (2013).

[23] A. Splendani, L. Sun, Y. Zhang, J. Kim, C.-Y. Chim, G. Galli, and F. Wang, Emerging photoluminescence in monolayer MoS_2, Nano Lett. **10**, 1271 (2010).

[24] Y. Li, Y. Rao, K. F. Mak, Y. You, S. Wang, C. R. Dean, and T. F. Heinz, Probing symmetry properties of few-layer MoS_2 and h-BN by optical second-harmonic generation, Nano Lett. **13**, 3329 (2013).

[25] S. Shree, D. Lagarde, L. Lombez, C. Robert, A. Balocchi, K. Watanabe, T. Taniguchi, X. Marie, I. C. Gerber, M. M. Glazov, L. E. Golub, B. Urbaszek, and I. Paradisanos, Interlayer exciton mediated second harmonic generation in bilayer MoS_2, Nat. Commun. **12**, 6894 (2021).

[26] A. Michail, N. Delikoukos, J. Parthenios, C. Galiotis, and K. Papagelis, Optical detection of strain and doping inhomogeneities in single layer MoS_2, Appl. Phys. Lett. **108**, 173102 (2016).

[27] M. Yamamoto, T. L. Einstein, M. S. Fuhrer, and W. G. Cullen, Anisotropic etching of atomically thin MoS_2, J. Phys. Chem. C **117**, 25643 (2013).

[28] Z. Y. Zhu, Y. C. Cheng, and U. Schwingenschlögl, Giant spin-orbit-induced spin splitting in two-dimensional transition-metal dichalcogenide semiconductors, Phys. Rev. B **84**, 153402 (2011).

[29] C. V. Nguyen, N. N. Hieu, D. Muoi, C. A. Duque, E. Feddi, H. V. Nguyen, L. T. T. Phuong, B. D. Hoi, and H. V. Phuc, Linear and nonlinear magneto-optical properties of monolayer MoS_2, J. Appl. Phys. **123**, 034301 (2018).

[30] T. Y. Ko, A. Jeong, W. Kim, J. Lee, Y. Kim, J. E. Lee, G. H. Ryu, K. Park, D. Kim, Z. Lee, M. H. Lee, C. Lee, and S. Ryu, On-stack two-dimensional conversion of MoS_2 into MoO_3, 2D Mater. **4**, 014003 (2017).

[31] H. Zhou *et al.*, Thickness-dependent patterning of MoS_2 sheets with well-oriented triangular pits by heating in air, Nano Res. **6**, 703 (2013).

[32] Y. K. Lin, R. S. Chen, T. C. Chou, Y. H. Lee, Y. F. Chen, K. H. Chen, and L. C. Chen, Thickness-dependent binding energy shift in few-layer MoS_2 grown by chemical vapor deposition, ACS Appl. Mater. Interfaces **8**, 22637 (2016).

[33] T. Yang, S. Sleziona, E. Pollmann, E. Hasselbrink, P. Kratzer, M. Schleberger, R. K. Campen, and Y. Tong, Isolating the optical response of a MoS_2 monolayer under extreme screening of a metal substrate, Phys. Rev. B **109**, L161402 (2024).

[34] X. Wang, W. Fan, Z. Fan, W. Dai, K. Zhu, S. Hong, Y. Sun, J. Wu, and K. Liu, Substrate modified thermal stability of mono- and few-layer MoS_2, Nanoscale **10**, 3540 (2018).

[35] B. Tang, H. Veluri, Y. Li, Z. G. Yu, M. Waqar, J. F. Leong, M. Sivan, E. Zamburg, Y.-W. Zhang, J. Wang, and A. V.-Y. Thean, Wafer-scale solution-processed 2D material analog resistive memory array for memory-based computing, Nat. Commun. **13**, 3037 (2022).